World Academy of Science, Engineering and Technology
International Journal of Computer and Information Engineering
Vol:6, No:8, 2012

A Robust Extrapolation Method for Curtailed Aperture Reconstruction in Acoustic Imaging

R. Bremananth

Abstract—Acoustic Imaging based sound localization using microphone array is a challenging task in digital-signal processing. Discrete Fourier transform (DFT) based near-field acoustical holography (NAH) is an important acoustical technique for sound source localization and provide an efficient solution to the ill-posed problem. However, in practice, due to the usage of small curtailed aperture and its consequence of significant spectral leakage, the DFT could not reconstruct the active-region-of-sound (AROS) effectively, especially near the edges of aperture. In this paper, we emphasize the fundamental problems of DFT-based NAH, provide a solution to spectral leakage effect by the extrapolation based on linear predictive coding and 2D Tukey windowing. This approach has been tested to localize the single and multi-point sound sources. We observe that incorporating extrapolation technique increases the spatial resolution, localization accuracy and reduces spectral leakage when small curtail aperture with a lower number of sensors accounts.

Keywords—Acoustic Imaging, Discrete Fourier Transform (DFT), k-space wavenumber, Near-Field Acoustical Holography (NAH), Source Localization, Spectral Leakage.

I. Introduction

NEAR-FIELD acoustical holography (NAH) is an essential method for acoustic radiation visualization and localization using discrete Fourier transform (DFT). However, due to small curtail aperture in conventional DFT-based NAH, there are several obstacles when reconstructing acoustical imaging is alarmed such as spectral leakage effect [1], acoustical deformation, poor regularization on wavenumber space (k-space) before inverse propagating and other artifacts. Our focus of this paper mainly belongs to reconstruct the acoustic sources with minimum spectral leakage effect when a small grid of sensors is utilized. William and Maynard [2] [3] introduced near-field acoustical holography for inverse determination of waveform patterns by means of holography. Arbitrary form of source areas such as cylindrical, spherical and other sources is reconstructed by applying DFT-based NAH, a complete reference in described by E.G. Williams [4].

Two-dimensional (2-D) DFT and its inverse transform are employed with Green's function propagating factor to reconstruct the measured acoustic source. Normally, in order to avoid reconstruction problems, DFT-based NAH requires a ratio of 4:1 between measurement and source apertures. But, in practical implementation, it is more expensive of a large grid of sensors [5]. Alternatively, when we employ a small curtailed aperture with less number of microphones that increases reconstruction errors, particularly in the edge of measurement aperture, due to spectral leakage effect of DFT. In order to avoid the problem of DFT-based NAH and extend reconstruction to arbitrary surfaces, produce a quite number of research works using alternative solutions such as statistically optimized NAH (SONAH) [6], boundary element method NAH (BEM-NAH) [7] and Helmholtz equation least-squares (HELS) [8] methods. Currently there are many other acoustic holography methods suggested for localizing point and planar sources in [9] [10]. A method proposed by Steiner et al. removed entirely the usage of k-space and DFT [11]. An iteratively based extrapolation for virtually enlarging the measurement plane was proposed by E.G.Williams [9]. In this method k-space regularization and zero-padding were collectively used to suppress high wavenumber leakage, iteration process was repeated until a specified threshold is not expected. It provided good results for well-known sources and pre-defined environments whereas active-region-of-sound (AROS) are unknown with sufficient amount of noise or other deformation such as an industrial situation, it could fail to perform well. SONAH is another substitution to the DFT-based NAH by using spatial convolution to calculate back-propagation between measurement and assumed virtual source apertures. However, SONAH requires a long-term computation due to its spatial domain convolution process to determine the inverse solution for the acoustical source reconstruction. In this paper, we propose a simple and an efficient DFT-based NAH using least-square predictive coding (LSPC). The proposed method makes DFT-based NAH as a powerful tool even for a small curtail aperture and reduce the localization error particularly near the boundary edges. Main idea behind in this method is to virtually enlarge the measured curtail aperture before DFT is applied. It ensures that minimal distortions occur in close to proximity of edges and reduce the high spectral leakage in k-space. This method triggers to pad the acoustic data from the known data of the measurement aperture to the unknown outward curtailed aperture based on linear prediction, while existing measured curtail aperture is remained unchanged.

The remainder of this report is organized as follows. Section II summarizes the basics of acoustical holography and its related problems. Proposed methodology of extrapolation is emphasized in Section III. The experiments and simulation results are shown in Section IV. Section V describes the concluding remarks and future research directions.

Ramachandran Bremananth is with the Information Systems and Technology Department, Sur University College, Sur, Sultanate of Oman, Affiliated with Bond University, Australia. He can be reached at bremresearch@gmail.com or bremananth@suc.edu.om (Let you know more, see http://www.suc.edu.om).

II. Basics of Fourier Acoustics and its Problems

In planar acoustical holography, a 2-D grid of sensor/micrphones are used for measuring sound source and the

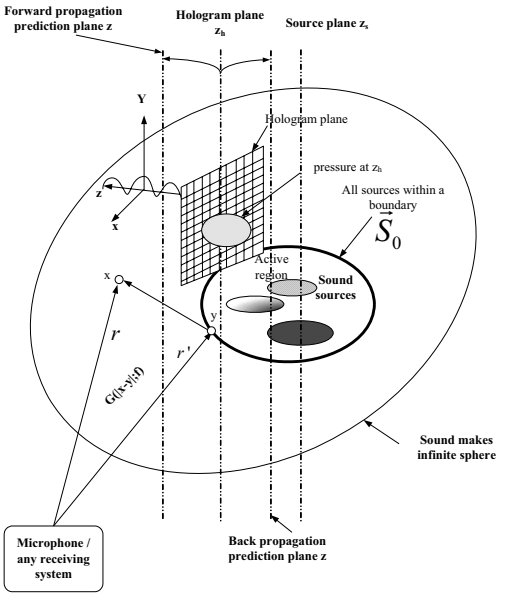

Fig. 1. Illustration of basics of acoustic holography.

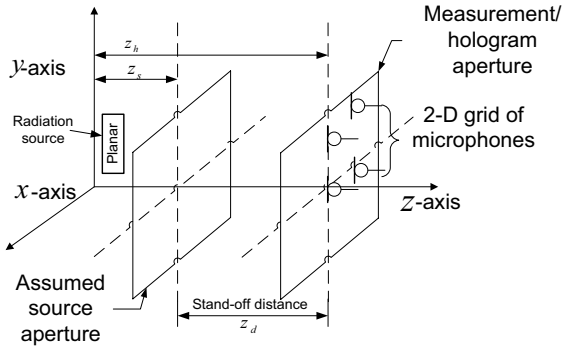

Fig. 2. A coordinate system of NAH, distance from an origin and source aperture z_s, from source aperture to measurement aperture z_h and stand-off distance z_d.

measured sound is back propagated to the assumed source aperture for reconstruction. A measurement aperture is also referred as a hologram aperture that has all necessary information to estimate the unmeasured acoustic values such as pressure, velocity, intensity, potential and kinetic energy. Figure 1 shows the basics of acoustical holography, where $\overrightarrow{S_0}$ denotes a boundary of the sound within this region active sound radiates. z_s and z_h represent source and measurement/hologram aperture, respectively. When sound is propagated in air then an infinite sphere is formed. As such fixing a boundary condition is an essential to estimate the sound source based on Green's function $G(\|\mathbf{s}-\mathbf{m}\|, f)$. This is used to solve boundary conditions either in the form of Dirichlet or Neumann that expresses how sound radiates from a point of source to destination. This is described as

$$\begin{aligned} \mathbf{s} &= [s_x\ s_y\ s_z]^T, \\ \mathbf{m} &= [m_x\ m_y\ m_z]^T, \\ G(\|\mathbf{s}-\mathbf{m}\|, f) &= \frac{1}{4\pi\|\mathbf{s}-\mathbf{m}\|} e^{(ik\|\mathbf{s}-\mathbf{m}\|)}, \end{aligned} \quad (1)$$

where f , $\mathbf{s}$, $\mathbf{m}$, and k denote respectively, frequency of the sound, the source location, microphone/sensor position, and wavenumber $k = \frac{2\pi f}{c}$, while c represents sound propagation speed.

Figure 2 illustrates a typical coordinate system of NAH with radiation planar source, assumed source z_s and measurement apertures z_h. Measured sound source is inversely back propagated to the assumed source aperture located at z_s with stand-off distance z_d in order to reconstruct the true sound source.

A. Basics of radiation sound source

Rayleigh integral is an essential method to estimate the sound pressure of the source It is employed by treating the source as an infinite number of radiating points. A point source can be envisioned as a minute sphere vibrating with angular frequency $\omega = 2\pi f$, which can be calculated by multiples of wave frequency f. The spherical pressure around the source is specified by

$$p = \frac{A}{r} e^{j(\omega t - kr)}, \quad (2)$$

where p is the radiated sound pressure which is going to be estimated, A is the amplitude of the vibration on the surface, $r = \|\mathbf{s}-\mathbf{m}\|$ is the distance between the source and measurement aperture, k is the wave number, j is the unit complex number in the space and t denotes the time. Certain assumptions are required for implementing Rayleigh integral in the source prediction. The assumptions are such as source must be planar and is surrounded by rigid infinite confound [12] [4]. First assumption is required for integrating Rayleigh integral to the source aperture. The second one is necessary that back propagation is executed on the front side of the plane in order to estimate the sound pressure on one side of the source, i.e., other side of the aperture and noise sources are not considered. Based on these assumptions the Rayleigh integral has been depicted in Fig. 3 and predict the pressure by

$$p(x,y,z) = \frac{-i\rho_o ck}{2\pi} \int\int_s \dot{w}(x^{'}, y^{'}, z^{'}) \frac{e^{ik|r-r^{'}|}}{|r-r^{'}|} dx^{'} dy^{'}, \quad (3)$$

where s is the overall area of the measurement, $\dot{w}(x^{'}, y^{'}, z^{'}$ is a velocity of the source and ρ_o is a density of the material. The variables $x^{'}$, $y^{'}$, $z^{'}$ and $|r-r'|$ denote respectively, axes of the measurement aperture x , y, z and the distance between the source and measurement apertures. The speed of the sound is calculated by $c = \sqrt{C/\rho}$, where ρ represents density of the particle and C is a co-efficient of stiffness of the material. Therefore, the sound speed is directly related with the stiffness of the density. The summation of each differential area dx', dy' is used to compute the pressure at each point of the source [4] [13]. Sampling distance mainly depends on the distance between the source and measurement $|r - r'|$ apertures. A smaller distance determines less discrete spatial errors. In

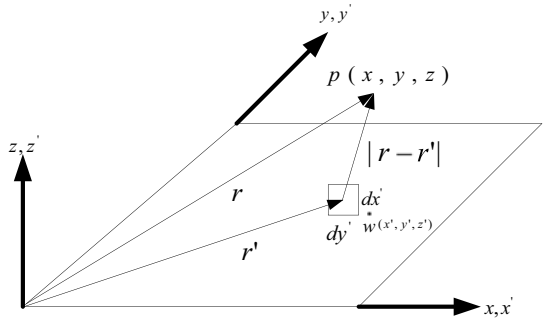

Fig. 3. Typical illustration of a geometry of Rayleigh integral [4].

order to avoid these errors, sensor spacing in the measurement aperture should be smaller than the distance between source and measurement plane [14].

B. Wave propagation

The basic idea of acoustic holography is based on propagation of waves. It is mainly dependent on the sound pressure $p(x, y, z; t)$ in different materials that satisfy the homogenous acoustic wave equation as

$$\nabla^2 p - \frac{1}{c^2}\frac{\partial^2 p}{\partial t^2} = 0, \tag{4}$$

where ∇^2 is the Laplace operator, p represents pressure on the acoustic plane. The variables c and t denote respectively, the speed of sound in the material and time-of-propagation. Cartesian coordinates of the Laplace operator is defined as

$$\nabla^2 = \frac{\partial^2}{\partial x^2} + \frac{\partial^2}{\partial y^2} + \frac{\partial^2}{\partial z^2}. \tag{5}$$

Eq.5 is often employed in the study of physical problems involving the partial differential in both space and time. In fluid dynamic, Euler's equation (6) governs flow of the fluid and assumed to be no stickiness, it represents the dependence of velocity on pressure of the material as [4]

$$\rho_0 \frac{\partial \vec{v}}{\partial t} = -\vec{\nabla} p, \tag{6}$$

where p , $\vec{v}$, ρ_0 and $\vec{\nabla}$ denote respectively, the pressure, velocity vector, fluid density and divergence operator in the vector field. A velocity vector consists of three components, i.e., $\dot{x}a+\dot{y}b+\dot{z}c$, where (a, b, c) , $\dot{x}$, $\dot{y}$, $\dot{z}$ represent respectively, unit vectors and forces at x, y and z directions. This is mainly based on Newton's law of motion, $Force = acceleration \times mass$, $mass = \rho_0 \Delta x \Delta y \Delta z$ and fluid density produces, $\rho_0 \frac{\partial \dot{x}}{\partial t} = -\frac{\partial p}{\partial x}$, this yields the same for other directions y and z as well. In the harmonic analysis, i.e., from the time to frequency domain, $p(r; t) = p(r; f)e^{-i2\pi f t}$, we can write the Helmholtz equation as

$$\nabla^2 p(r; f) + k^2 p(r; f) = 0. \tag{7}$$

The solution to (7) is Kirchhoff-Helmholtz integral [15]. The sound pressure and velocity are determined in all points on its surface $\vec{S_0}$ described as

$$p(r; f) = -\frac{1}{4\pi}\int_{\vec{S_0}} \left[G(r, r'; f)\frac{\partial p(r'; f)}{\partial n} - p(r'; f)\frac{\partial G(r, r'; f)}{\partial n} \right], \tag{8}$$

where $p(r; f)$, $p(r'; f)$ and n represent respectively, pressure to be predicted, pressure on source boundary $\vec{S_0}$ and the normal direction of the boundary surface. $G(r, r'; f)$ denotes Green's function of Dirichlet boundary condition that the partial differential conditions produce the value of the function $T = D(r'; t)$ on surface $\vec{S_0}$. In order to predict either p or $\partial p/\partial n$ in the planar acoustic holography, we can assume that r' and r turn out to be x_0, y_0, z_0 and x, y, z, where x_0, y_0, z_0 and x, y, z signify respectively, the origin of the source and any points on the hologram plane. If G is selected such that $G = 0$ on the source boundary S_0, then (8) can be rewritten as

$$p(x, y, z; f) = \frac{1}{4\pi}\int_{-\infty}^{\infty}\int_{-\infty}^{\infty} p(x_0, y_0, z_0; f) \frac{\partial G(x - x_0, y - y_0, z - z_s; f)}{\partial n} dx_0 dy_0. \tag{9}$$

Based on Fourier acoustic, NAH method is to be implemented. The problems associated with the acoustic inverse problems are necessary because they are important to understand the process of back propagation in the vibrating surface. Acoustic vibrations in solid structures essentially involve the propagation of wave motion through the material. Wavelength of harmonic wave is described as λ. This is called as the spatial period of a wave shown in Fig. 4. The phase change per unit distance is expressed as the spatial variation and this is referred as the wavenumber $k = \frac{2\pi}{\lambda}$ and $\lambda = c/f$. The wavenumber k has the magnitude of wavenumber vector (k_x, k_y, k_z) and indicates the phase variation speed of the propagation. Any spatial variation can be analyzed by wavenumber spectrum. Likewise, we can compute spectrum of temporal variations $\omega = 2\pi/T$ and $T = 1/f$.

C. Fourier Acoustic based Wavenumber

In DFT-based NAH, Fourier transform is an essential method for computing acoustic wave propagation between measurement and source apertures. DFT decomposes the signals into plane waves. The continuous Fourier transform is given as

$$F(k) = \int_{-\infty}^{+\infty} f(x)\left[\cos(kx) - j\sin(kx)\right] dx. \tag{10}$$

where $F(k)$, k, x and $f(x)$ represent respectively, Fourier coefficients, variable in Fourier space, original input variable and measured signal. Instead of using sinusoids, a common way

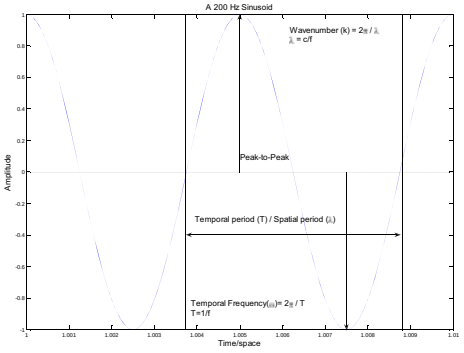

Fig. 4. Representation of temporal and spatial periods.

of representing the continuous form by the Euler's formula ($e^{(-jx)} = \cos x - j \sin x$) of (10) is as follows

$$F(k) = \int_{-\infty}^{+\infty} f(x) e^{-jkx} dx. \tag{11}$$

where $k = 2\pi/\lambda$ is the wavenumber, then (11) becomes wavenumber based Fourier transform and its inverse form is,

$$f(x) = \frac{1}{2\pi} \int_{-\infty}^{+\infty} F(k) e^{jkx} dk. \tag{12}$$

As per our previous discussion, in the vibrating surface Rayleigh waves are dominant therefore we assume that surface is flat and infinite stiff confound. Rayleigh integral can evaluate the sound power radiated by a vibrating surface. Generally, a convolution problem may appear in the Rayleigh integral for the acoustic wave propagation. It may be resolved by Fourier transform. That is, convolution integral in the space domain is equal to the multiplication in wavenumber domain. In wavenumber propagation, extend Eqs. (12) and (11) to 2-D discrete forms with $N \times M$ frequency rectangle as

$$F(k_x, k_y, z; f) = \sum_{n=0}^{N-1} \sum_{m=0}^{M-1} p(x, y, z; f) e^{-j(k_x n/N + k_y m/M)}, \tag{13}$$

$$p(x, y, z; f) = \frac{\left(\sum_{n=0}^{N-1} \sum_{m=0}^{M-1} F(k_x, k_y, z; f) e^{-j(k_x n/N + k_y m/M)} \right)}{NM}. \tag{14}$$

D. Plane and Evanescent Waves

Measured acoustical signal consists of plane and evanescent waves. Evanescent wave is a heterogenous short-lived wave whose amplitude decays exponentially from the source to measurement aperture and renders NAH in an ill-posed problem [4]. In addition, evanescent influences more control over the propagating wavenumber spectrum as shown in Fig. 5a.

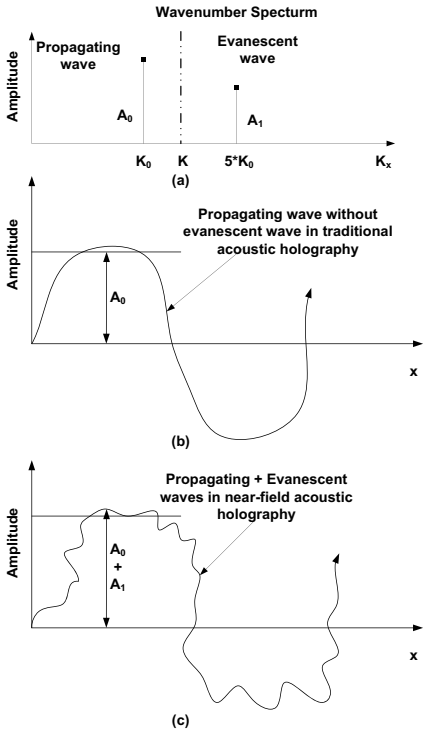

Fig. 5. (a) Wavenumber spectrum of plane wave (b) Traditional acoustic holography (c) Evanescent wave in near acoustic holography.

Whereas plane wave has no change in the amplitude as shown in Fig. 5b, the same case happen in the far-field acoustical holography also. We assume that a curtail set of sensors of the measurement aperture receive the approximately equivalent amplitude as the true sound source radiates from the source. However, in the NAH, due to evanescent waves not all sensors in the measurement aperture receive the acoustic signals as exact as the true source radiates. The deformation of receiving signals is illustrated in Fig. 5c. Therefore, when these waves are back propagated to the source, they should be amplified exponentially. Sensors of measurement aperture are received both plane and evanescent waves simultaneously from the acoustical source by satisfying Eq. (7). Assume that maximum wavenumber of the domain is $k_{max} = \frac{\pi}{\Delta}$, where Δ denotes sensor spacing and $k = \frac{2\pi}{\lambda}$. The plane waves turn into evanescent waves when k_x or k_y is greater than k_{max}, otherwise plane wave is related. The wavenumbers relationship and its errors will be discussed in the following section.

E. Wavenumber and Its Errors

As we discussed previously, Helmholtz Eq. (7) plays an important role in reconstructing the source. Wavenumber domain is essentially involved to meet the boundary conditions. We can define plane wave as

$$p(\omega) = A(\omega) e^{i(k_x x + k_y y + k_z z)}, \tag{15}$$

where k_x, k_y and k_z denote respectively, the directional wavenumbers in x, y and z directions. Acoustic wavenumber

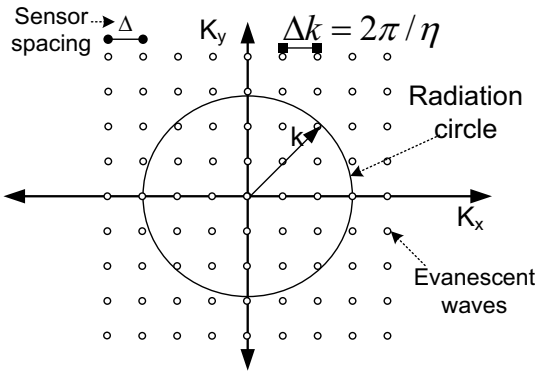

Fig. 6. Representation of plane wavenumber propagation with plane and evanescent waves.

k is defined as

$$\begin{aligned} k^2 &= k_x^2 + k_y^2 + k_z^2, \\ k &= \sqrt{k_x^2 + k_y^2 + k_z^2}. \end{aligned} \tag{16}$$

By using z-direction as the dependent, we can rewrite (16) viz

$$k_z = \pm\sqrt{k^2 - k_x^2 - k_y^2}. \tag{17}$$

Directional wavenumbers k_x, k_y and k_z in (15) satisfy (17), when wavenumbers of x or y directions greater than k then the plane wave turn into the evanescent wave. The followings are the conditions of plane and evanescent waves

Condition 1: If $k^2 \geq k_x^2 + k_y^2$ then $k_z = \sqrt{k^2 - (k_x^2 + k_y^2)}$ and k-space points are within the radiation circle as shown in Fig. 6. It represents the plane wave with directional wavenumbers k_x, k_y, and k_z, with k_z real. In this criterion, wavenumber domain is not involved for considering short-lived evanescent waves.

Condition 2: Else if $k^2 < k_x^2 + k_y^2$ then $k_z = i\sqrt{(k_x^2 + k_y^2) - k^2}$, k-space points are outside the radiation circle and plane waves are treated as evanescent waves. k_z is an imaginary number. This decisive factor is employed for localizing radiation sources with the minimum distance variations. In this criterion, we specify the minus sign to represent the back propagation of plane waves towards the source in order to localize an AROS.

Condition 3: If $k_x^2 + k_y^2 = k^2$ then k-space points coincide exactly on radiation circle, the plane waves are propagating in z-direction and DFT could fail to do prediction. It may be $k = 2\pi/\eta$ minimum failure, where η is one wavelength across the aperture, if $\lambda = \eta$ [16]. Resolution of source reconstruction using NAH mainly depends on the wavenumber resolution. It is determined by the size of the aperture in the measurement. In order to localize entire source, inclusive of the aperture edges and its derivatives, a method based on zero-padding based on windowing was suggested before DFT is applied [7]. An application of large-scale reconstruction is a challenging process when measurement aperture is smaller than the source. It is assumed that, in NAH signal processing, acoustic signals are measured using limitless size of sensors in order to reconstruct entire radiated sound source. However, in practice, usage of large-size of sensor is an expensive one and produces more computational complexity in the reconstruction. This restriction causes wraparound error and curtail aperture. Wraparound errors are mainly due to spectral leakage effect of curtail aperture by applying DFT and its frequency bins limitations. Generally, padding zeros outside the measured aperture reduce the spectral leakage by assuming that radiating source sound outside measurement aperture is negligible.

F. Finite Aperture Problem

In NAH, a finite number of sensors is utilized to reconstruct acoustic sources. Due to the discrete Fourier transform over the finite measurement points, the prediction of sources have the wraparound errors. However, these errors can reduce by sufficiently enlarge the aperture by applying zero signals other than measured part of the signals. A discontinuity of signal variation between the actual measured acoustic and the padded zero signals, this discontinuity intensifies at the aperture edges in the back-propagation [17]. As a result of reconstruction, discontinuity of measurement aperture is deformed especially over the edges. In order to reduce this deformation, windowing is applied appropriately to the synthesized zero-padded aperture. Due to tapering value and multiplication of windowing, the measured signal of measurement aperture is changed significantly. The application of window produces more errors on the measurement aperture. Conservatively, in order to reduce the reconstruction error as per signal processing, the measurement aperture should be infinitely larger than the radiating surface. For practical applications, however, this is often prohibitive due to constraints pertaining to the size of aperture as well as computational complexity. In addition, a finite measurement is processed by a rectangular window function. They are mainly employed to determine the quality of data acquisition during the measurement. We can define a spatial rectangular function in x and y directions as,

$$R_x(x) = \begin{cases} 0, & \text{if } |x| > W_x/2, \\ 1/2, & \text{if } |x| = W_x/2, \\ 1, & \text{if } |x| < W_x/2, \end{cases} \tag{18}$$

$$R_y(y) = \begin{cases} 0, & \text{if } |y| > W_y/2, \\ 1/2, & \text{if } |y| = W_y/2, \\ 1, & \text{if } |y| < W_y/2, \end{cases} \tag{19}$$

where R_x, R_y, W_x and W_y denote respectively, spatial rectangular function in x,y directions, spatial interval width in x and y directions. In addition to the time discretization sampling, an acoustic imaging of the discrete system requires spatial sampling to the finite number of sensor positions with the finite spatial intervals. The impulse train function used to represent

spatial sampling in the acoustic imaging is

$$\begin{aligned} I(x) &= \sum_{n=-\infty}^{\infty} \delta(x - x_n), \\ I(y) &= \sum_{m=-\infty}^{\infty} \delta(y - y_m), \end{aligned} \tag{20}$$

where $\delta()$, $I(x)$, $I(y)$, x_n and y_m represent respectively, Dirac delta function, impulse train functions in x and y directions, spatial discrete coordinates in x and y directions. Using (18), (19) and (20), we can describe the pressure as

$$p(x_n, y_m) = p(x, y)R_s(x)R_s(y)I(x)I(y). \tag{21}$$

Finite boundary of the measurement aperture in k-space can be computed based on the angular spectrum as

$$p(k_x, k_y, z_h) = \sum_{n=0}^{N-1} \sum_{m=0}^{M-1} p(x_n, y_m) e^{-j2\pi(k_x n/N + k_y m/M)}. \tag{22}$$

Discrete solution to the wave equation in k-space can be written as

$$p(k_{xn}, k_{ym}, z) = p(k_{xn}, k_{ym}, z_h) e^{jk_z(z - z_h)}. \tag{23}$$

As per our previous discussion, In k-space, k_z is determined by (17), It can provide a solution for plane waves, $k_x^2 + k_y^2 = 0$ and $k_x^2 + k_y^2 \leq k^2$ denote respectively, plane waves in z-direction and $k_z$is real. Evanescent waves components are represented by $k_x^2 + k_y^2 > k^2$ and k_z is imaginary.

If propagation constraints apply to the discrete wave Eq. (23) then it reveals the phase shift as a result whereas in k-space, evanescent waves are amplified through multiplication with an exponentially increasing power of k_z. For this reason, before performing DFT and wavenumber operations over the measured hologram data, we possibly do the spatial preprocessing. There is no direct sampled data of the sound field outside the measurement aperture as illustrated in Fig. 7. Consequently, the k-space is also resolved from the ill-posed, spatially sampled and finite aperture problems. The choice of a windowing function is scrutinized as a procedure to diminish the order of the discontinuity at the edge of the intermittent extension of the aperture. The edges over the hologram plane can be estimated either by smoothly attenuating the data near the edges to zero or extrapolating sampled data on the partially sampled regions. Furthermore, we have to estimate the unknown acoustic signal outside of the hologram aperture. If the wavenumber of N basis set of intervals is defined then there exists a signal in the defined set with a wavenumber not exactly fitting on one of the basis [1]. The windowing function transforms this signal to the basis wavenumber closest to the original wavenumber of the signal, therefore, k-space spectrum resolution is low. The discontinuous edge between aperture and measured area indicates the presence of non-appropriate intermittent signals. It causes leakage of wavenumber spectrum. This means that only ill-posed aperture data are available and an important process should be involved to determine the suitable k-space with as much conserved spatial data as possible. In addition to that, it implies a relationship between the amount of k-space leakage and loss of acoustic pressures, principally in close proximity to the edges. If a large aperture size with more sensors in involved, then less amount of localization errors will occur. Whereas we utilize a small aperture with less number of sensors, it causes larger errors with respect to wavenumber leakage, inaccurate localization and other deformations, specifically around edge area. A method is required to pad the acoustic data in the borders of the hologram plane outward, while the true acoustic measured data is remain unchanged. It tends to localize the source with minimum number of leakage at the k-space domain.

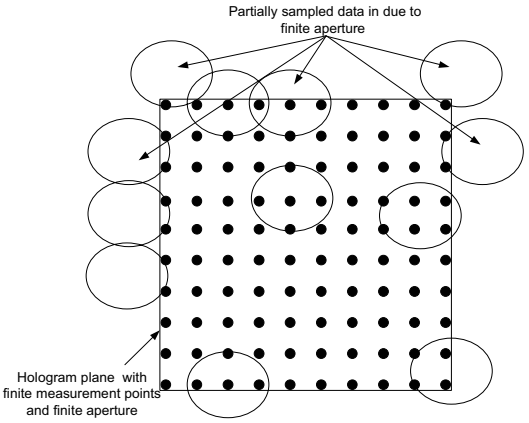

Fig. 7. Finite aperture and partially measured data at hologram plane.

G. Zero-padding Problem

In order to interpolate among the basis of wavenumbers, we can possibly utilize zero-padding on the edges. The edges and all of its derivatives in the neighborhood is set to zero. So that, we can apply DFT on the zero-padded spatially sampled data to get the k-space spectrum. It causes free of periodic image at the wavenumber spectrum. Nevertheless, due to the finite number of sampling points, we can make discrete wavenumber bins available to map the data on the measurement aperture. The discrete k-space is a conspiring of the continuous spectrum on the set of available basis of k-bins in the wavenumber domain. It has the remaining set of unknown spatial data in k-space to exactly match the discrete of the wavenumbers due to its periods. An imperfect resolution occurred in k-space is mainly due to finite length of the spatial aperture. We extrapolate the new samples with zero value then it increases the spatial aperture and computing complexity of the DFT. For example, if every single portion increases higher than the actual aperture size then it reflects the numbers of bins b in k-space as $k = 2\pi/(N+b)$. A greater number of wavenumbers are distinguished from the spectrum. Even though the zero-padding may not increase the spectral resolution in k-space, it can increase the spatial resolution over the measurement plane alone. On the other hand, by expanding the N samples by n samples, it demands $O(N +$

$n \log N + n)$ computational complexity. Moreover, it is notable that assumption of padding zeros on unmeasured acoustic field does not increase spectral resolution on wavenumber domain. A one-dimensional linear prediction algorithm proposed to estimate acoustic signal outside the measurement aperture [1]. However, in order to increase spectral resolution, we require an efficient method to estimate the unmeasured acoustic signal outside the measurement aperture.

H. Aliasing in Estimating Pressure

Aliasing refers to the effect which causes different signals to be indistinguishable i.e., aliases of one another, when sampled. It is also referred as the distortion happened when consequences of the reconstructed signals are different than the discrete samples and the original continuous signals. The effect of anti-aliasing makes the signals to be more distinguishable. In order to avoid aliasing during the measurements, we have to properly place the sensor with a suitable distance between them. For that, the Nyquist sampling rate is considered, which is a minimum sampling rate needed to avoid the aliasing [14]. This rate is normally the double of the highest frequency h_f of non-zero sound pressure contained in the measured signal, i.e., $N_r = 2h_f$. In general, sampling can be temporal sampling (time domain) or spatial sampling (space domain). In the former, sampling is in time Δt and the Nyquist frequency is computed as $N_f = 1/2\Delta t$. Whereas in the latter, sensor separation distance is Δ and Nyquist wavenumber becomes $N_k = \frac{1}{2}\frac{2\pi}{\Delta} = \frac{\pi}{\Delta}$. If measured signal frequencies are higher than the Nyquist frequency then it will fold back to the lower frequency. In order to distinguish spatial signals properly among the sensors, we have to avoid the spatial aliasing among the wavenumbers, which means that constraint $N_k > k$ should be satisfied thus the minimum sensor space as $\Delta = \lambda/2$, where λ denotes the wave length of a propagating wave.

In NAH, signal measurements are based on the discrete sampling system and is also affected by the errors due to discrete measurements. In order to avoid aliasing between the sensors at hologram plane, we are in need of utilizing the Nyquist wavenumber constraint. Furthermore, sensor separation distance Δ should also be less than the distance between measurement and source m_d, aperture as $\Delta < m_d$. For example, if a wave length of the sampling space is $\lambda = 0.1$ then sensor spacing becomes $\Delta = 0.1/2 = 0.05$ m. We assume that a hologram is required with signal-to-noise ratio of 60dB and the spatial resolution as 0.05 m, then measurement distance is computed as $m_d < (0.05 * 60)/27.2875271(20 * pi * log(e))$ $= 0.1099 \approx 0.1$ and sensor spacing should have a constrain of 0.05 m < 0.1 m.

III. Extrapolation of Curtailed Aperture

Structural vibration and sound radiation have related in prediction process of acoustic holography. Vibration passes on solids as a basis whereas sound radiation is created as a consequence. If basis is characterized, then the consequence is going to be predicted based on the vibration structural model. This is known as forward prediction. However, in the inverse prediction, the consequence is recorded and basis is going to be computed, that is, measuring the sound and predicting the source. This is referred to as inverse prediction. Due to the inadequate and incompleteness, the latter becomes ill-posed problem which is more complicated than the former. Based on these phenomena, our approach is employed for reconstructing vibrating sound sources. The challenge of this method is to localize sound source exactly at edges of aperture. Based on our previous discussion, a significant part of the edges in measurement aperture is affected by windowing. In order to reduce the large error, it is necessary to virtually enlarge the measurement aperture and avoid discontinuity of signals at the edge of measurement aperture. This further ensures the smooth transition of data between synthesized aperture and measured aperture without altering data true measured acoustic signals. An approach of spatial preprocessing is incorporated with the existing method of traditional NAH. The measured true 2-D acoustic signals $p(x, y, z_h; f)$ in the spatial domain are transformed into wavenumber domain by means of angular spectrum as $p(k_x, k_y, z_h; f)$. Before transforming a spatial preprocessing is performed as shown in Fig. 8. This spatial preprocessing is mainly used to enhancing the measurement aperture and makes it suitable for 2-D Fourier transform in order to reduce the spectral leakage. In addition, a regularization is required on k-space data as a post-processing to exerting influence the inversely propagated wavenumbers in order to achieve better inverse Fourier coefficients. Subsequently, it intends to increase accuracy of reconstruction. In order to reconstruct the source field at $z_s = z_h$, wavenumber pressure is multiplied by inverse propagator factor, $e^{-jk_z z_d}$. Wavenumber coefficients are inverse transformed as $p(x, x, z_s; f)$.

In our approach, we have used zero signals to fill the non-sampled area which occur in the neighborhood of the edges and derivatives.

A. Choosing Coordinate and Hologram Grid

In planar geometry, rectangle coordinate system is mostly preferred. Once it is chosen, we can make hologram grid surface. The span of the hologram plane is defined as h_n and h_m, the size of the sensor grid denoted as S_N and S_M and then the sampling interval can be calculated. In order to prevent aliasing problem, the sensor spacing should be less than the half of the wave length and the measurement distance between the hologram and prediction planes. This is because large sensor spacing will cause the insufficient spatial sampling and introduce aliasing in the prediction. Once the sensor spacing and measurement size are specified, the total measurement points can be determined. Furthermore, in planar NAH, the size of the aperture should be a power-of-two, normally, 2^2 times as size as the source surface so that adequate signals can be received to localize entire active sources. For example, a spatial resolution is calculated based on the wavelength of the vibrating structure, if the spatial resolution τ is 0.06 m, then minimum wavelength λ of the vibrating surface is $\tau = \lambda/2, 2*0.06 = 0.12$ m. Since acoustic spatial discretization are determined we require a minimum number of nodes per wavelength. This is the case consider in the experiment. In the next section, we discuss the setting signal parameters and extracting single frequency.

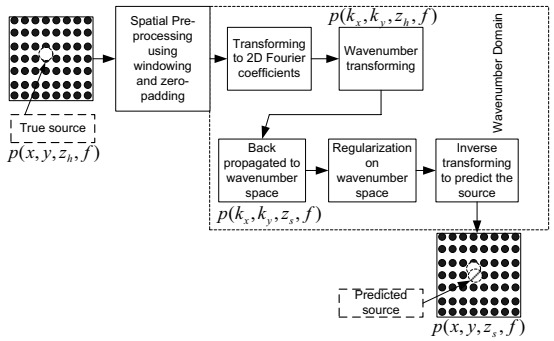

Fig. 8. Overall flow of the NAH in localization.

B. Setting Signal Parameters and Extracting Frequency

Setting up the signal parameters is an essential task for free-field environment. The procedures are as follows, define the reverberation time $R_t = cv/s_s a_c$, where c, v, s_s and a_c denote respectively, speed of the sound in the environment, the volume of the room, total surface area of a room, and the average absorption coefficient of room surfaces. Signal speed is defined based on the type of vibrating structure which we are using for the application. Furthermore, it can also be defined based on modulus of elasticity, Poisson's ratio, density kg/m^3 and coefficient of absorption. After that sampling frequency f_s has been specified.

If a source is radiate a single time frequency pressure field then all the sensors in the measurement plane will capture a signal having this time frequency. So that, in order to extract the single frequency, the time series recorded by each sensor are transformed into Fourier coefficients. Then we find the index of maximum coefficient of the fourier spectrum of each sensor, and fetch the median number of these indexes to be the frequency that we want to extract. Then, coefficients are directly chosen according to this index,and then multiplied with the corresponding exponential term. Generally, considering the Nyquist theorem, the sampling frequency should be twice the frequency of the signal. For this reason, we will only consider the the frequency-span in the first half of the transformed spectrum.

This method could fail due to the dependence of peak amplitude of Fourier spectrum and finite aperture problems. furthermore, extraction of median frequency is not always the case in the practical implementation among the entire sensors of the measurement plane. It has the computational complexity of $o(n_2 \times Nlog(N))$, where n and N denote respectively number of sensors and length of data recorded by each sensor in the measurement plane.

That's why, we propose single frequency extraction approach based on the configuration of measurement plane. Here, in accordance to the touch acoustic wave and measurement plane's wavenumbers, single frequency has been extracted. In this method, we find the best frequency that is suitable for a measurement plane, with a specific aperture size and sampling space to capture. For example, we have an aperture size A_m and N_s sensors have been utilized for measurements then we assume that the largest wavenumber of the pressure field can be represented without aliasing is as

$$k_{max} = \pi/\Delta, \tag{24}$$

where Δ is sensor spacing. We assume that a suitable wavenumber contains same amount of evanescent wave and propagating wave. That is, the acoustic wavenumber should be

$$k = \frac{k_{max}}{2} = \pi/2\Delta. \tag{25}$$

And the acoustic wavenumber can also be calculated by

$$k = 2\pi f/c, \tag{26}$$

which means that

$$2\pi f/c = \pi/2\Delta. \tag{27}$$

Thus we can find that the suitable frequency should be

$$f = (\pi c/2\Delta)/2\pi = c/4\Delta. \tag{28}$$

Thus we can extract the suitable frequency. And $o(1)$ is the computational complexity alone. In practice, after this frequency, which we will later used for back propagation, is extracted, we can then determine the suitable sampling frequency of each sensors. which can be set as thrice as $3f = 3(c/4\Delta)$.

C. Localization of Touch Impact

Touch impact Localizing is a process to exactly locate the AROI among other coarse of the poses. Normally, the NAH computes intensity field of radiated sources. As per our work is concerned, we aim to develop a system to localize the finger impacts as an AROI. The intensities of impact are measured to locate the peak amplitude of the touch source. However, a main challenge of NAH is that it treats the source of sound as stationary and localize the sources entirely dependents on the size of the aperture. We numerically simulate the touch impact source. Fig. 9 shows its impulse responses. Once an environment is formed, the finger taps amplitudes have to be filtered according to impulse response of the environment. This is shown in Fig. 10. It reveals that impact of the finger may have different size and amplitudes. The amplitudes variations depend on the force of the finger tapping on the surface and also distorted by different kinds of external artifacts such as room temperature, noises, reflection media and other factors. Due to these factors, sensors in the measurement plane may receive distorted signals. From these amplitude variations of signals, exactly locating an impact is a difficult task. Especially, in the application of human-computer interaction, most of the factors would produce the inaccurate localization in the finger touch or drag. Due to various artifacts, predicted source in the back propagation may not be the same as true finger impact position. In this work, localization has been performed over the finger impact and predict the true source using complex k-space. In that, DFT has been performed on measured signals with wavenumber

filter and obtained coefficients of regularized hologram plane. These coefficients are back propagated to the prediction plane. It is based on the inverse DFT with wavenumber filter. Once finding the peak among the inverse coefficients, we can treat that peak inverse coefficient as an active region touch impact on the surface.

D. Increase the Spatial Resolution using Zero-padding

In connection with our previous works [18] [19], in this is research paper, we enhance the spatial resolution of the curtail aperture. Normally, due to the finite length of the spatial aperture, a fixed amount of resolution is appeared in the k-space. In order to increase the k-space resolution in both spatial and spectral, zero-padding is mainly performed for extrapolating a new pieces of samples with zero values. In addition, the prediction wraparound errors which occur in the inverse Fourier transform are also minimized by padding the zero samples hence the size of the hologram plane h_m,h_n becomes twice as the size as the hologram plane.

The partially sampled signals are synthesized by the zero samples in close to the edge positions by enlarging the hologram data virtually. Sampled data of the measurement plane is synthesized as (29), (30), (31) and (32) represent z_1, z_2, z_3 and z_4 regions of zero-crossing in the counterclockwise direction, respectively,

$$z(z_m,z_n)_{(z_m/2)\cdots h_m,(z_n/2)\cdots h_n} = \begin{cases} p(h_m,h_n), & \text{if } h_m > (h_m/2)\ and\ h_n > (h_n/2), \\ 0, & \text{otherwise} \end{cases} \quad (29)$$

$$z(z_m,z_n)_{(z_m/2)\cdots 1,(z_n/2)\cdots h_n} = \begin{cases} p(h_m,h_n), & \text{if } (h_m/2) > 1\ and\ h_n > (h_n/2), \\ 0, & \text{otherwise} \end{cases} \quad (30)$$

$$z(z_m,z_n)_{(z_m/2)\cdots 1,(z_n/2)\cdots 1} = \begin{cases} p(h_m,h_n), & \text{if } (h_m/2) > 1\ and\ (h_n/2) > 1, \\ 0, & \text{otherwise} \end{cases} \quad (31)$$

$$z(z_m,z_n)_{(z_m/2)\cdots h_m,(z_n/2)\cdots 1} = \begin{cases} p(h_m,h_n), & \text{if } h_m > (h_m/2)\ and\ (h_n/2) > 1, \\ 0, & \text{otherwise} \end{cases} \quad (32)$$

where $z(z_m,z_n)$ and $p(h_m,h_n)$ denote respectively, synthesized plane and measurement plane. In real practice, while localizing AROI at the edges, it is an essential to expand the measured aperture and ensure that AROI is not positioned in close proximity to the perimeter of the edges. However, our approach is able to localize sources near to the perimeter of the measurement plane and makes the smooth transitions without misplacing the original measured signals. This synthesizing method mainly deals with appending the samples with zeros but not predicted signals are padded in the derivative regions. For that, we require a method which predicts the pressure at non-sampled regions instead of simply padding with zeros. Nevertheless, this method enhances the resolution on hologram plane especially at discontinuity of non-sampled boundaries.

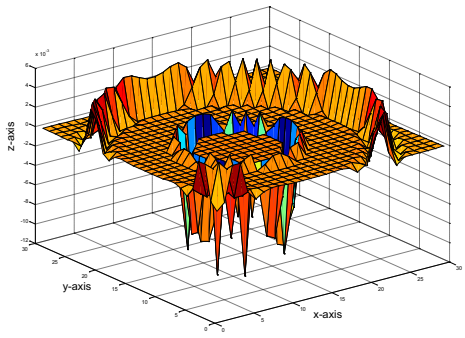

Fig. 9. Impulse response of the source with multi channel single response filter.

E. Wavenumber Transforming

In this section, complex wavenumber is utilized for locating AROIs using [18]. The synthesized plane is used for transforming measured pressure into Fourier coefficients. The size of the wavenumber is determined based on the synthesized plane as, k_n, k_m and generate linearly spaced vectors for structural wavenumbers viz $\Delta k_x = \frac{\pi}{z_m \Delta}$ and $k_x = (-\frac{z_m}{2}, -\frac{z_m}{2}+1, ..., \frac{z_m}{2}-1) \times \Delta k_x$, and $\Delta k_y, k_y$ is the same.

Perform FFT over synthesized zero-padded data and compute Δ_{dx} and Δ_{dy} for wavenumber spacing between x and y directions respectively as

$$\Delta_{dx} = (2\pi/\Delta_x)/z_m, \quad (33)$$

$$\Delta_{dy} = (2\pi/\Delta_y)/z_n, \quad (34)$$

where Δ_x and Δ_y represent sensor spacing in x and y directions of the synthesized plane respectively. In order to do the wavenumber transforming and inverse propagation, the following operations are performed as follows

$$k_{pro} = k^2, \quad (35)$$

$$k_x = \Delta_{dx}(k_{xi} - 1), \quad (36)$$

$$k_y = \Delta_{dy}(k_{yi} - 1), \quad (37)$$

$$k_{xy} = k_x^2 + k_y^2, \quad (38)$$

$$(39)$$

$$p(k_x,k_y) = \begin{cases} k_z = \sqrt{k_{pro} - k_{xy}}, & \\ z(z_n,z_m)e^{(ik_z z_d)}, & \text{if } (k_{pro} >= k_{xy}), \\ k_z = \sqrt{k_{xy} - k_{pro}}, & \\ z(z_n,z_m)e^{(k_z z_d)}, & \text{otherwise} \end{cases} \quad (40)$$

where $p(k_x,k_y)$ and $z_d = z_h - z_s$ denote wavenumber coefficients, the distance between hologram and source, respectively.

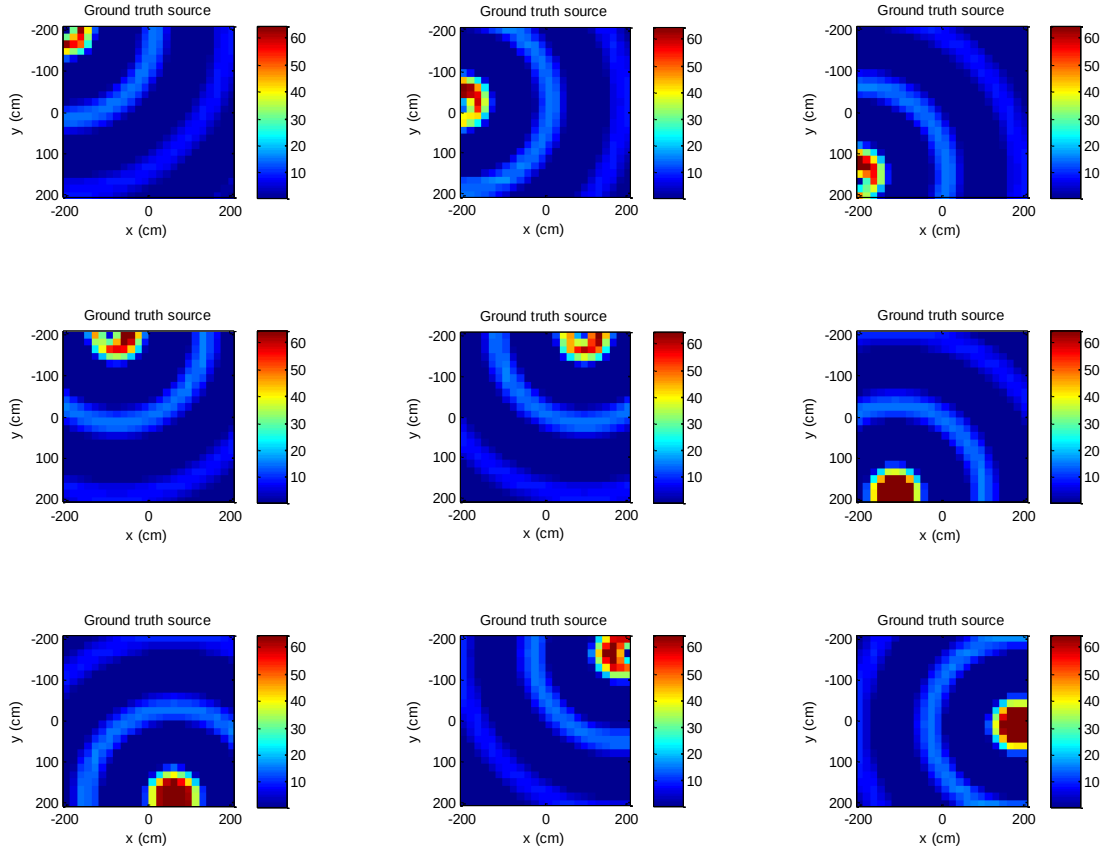

Fig. 10. Ground truth sources, z_d = 0.2m, 12 x 12 measurement positions and linear interpolation with 24 x 24.

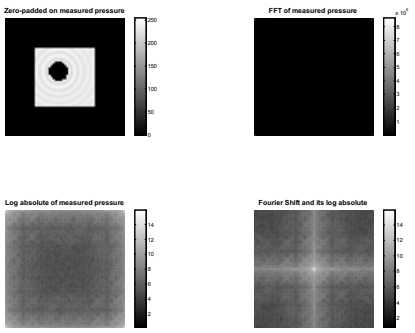

Fig. 11. Synthesized sampled plane and its Fourier transforms.

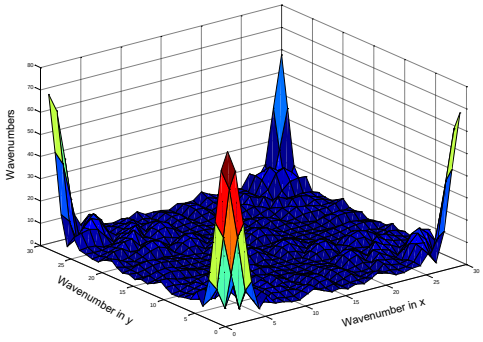

Fig. 12. Wavenumber response in real and complex k-space.

After wavenumber transforming, backward propagation and inverse FFT are carried out to localize the AROIs.

Naturally, a kind of jagged truncation is produced by the finite aperture. It causes impractical wavenumber artifacts. The high wavenumber artifacts have minimized by applying 2D-windowing with zero-padding. This process minimizes the discontinuity of non-periodic signals and high wavenumber artifacts. It ensures the smooth transition of data between measured data and padded zeros. Furthermore, we can extend this process in the inverse prediction to avoid the magnification of errors occurred in the evanescent components due to exponentially decaying in the localization.

Because of spatial preprocessing, the resolution of source localization will be improved and source near the edge of

measurement plane can be predicted rather accurately as well. Here, The whole wavenumber space, propagating or evanescent is employed for localizing impact point source. The spatial FFT is used for the prediction process, in that, transformed pressure coefficients are computed by exponential of k_z and z_d. This has been carried out, if k-space points are within or on the radiation circle. If k-space points are outside the radiation circle then pressures coefficients are calculated by exponential of inverse complex-space, k_z and z_d. Fig. 11 shows the zero-padded and wavenumber transformation using FFT. After transforming the zero-frequency components are collected to the center of the plane to evaluate the frequency variation among the measured pressure. The wavenumber response of the pressure coefficients are computed and their absolute deviations are studied. This is depicted in Fig. 12. It shows that transforming coefficients in complex space domains (evanescent) is essentially involved in predicting the sources of the entire surfaces regions.

Inverse transformation is carried out for back propagating the measured signals. After inverse transforming, a recovering zero-padding module has been invoked to get back the true pressure in order to retrieve the unmeasured data from the measured data set. During the experiments, the average peak-signal-to-noise ratio was around 15dB. To do the retrieving phenomenon, we could do the computation on wavenumber domain before performing the inverse transform. In the inverse problem, the propagator amplifies the high spatial frequency evanescent waves as the sound field which is to be propagated back towards the source. Due to spatial noise, wavenumber has a peak content but it not related with the spatial data. Furthermore, during the measurement, true pressure may convolve by spatial noise due to the factor of evanescent wave as a source in propagation plane. The sources of noise may include position of microphone, calibration, mismatches and other random sources. In order to tackle the evanescent wave, complex k-space would have been comprised in localizing source point. If the real k-space is single-handedly incorporated then the wavenumber domain has considered for the propagating wave alone so that wavenumber in the imaginary part abandoned from the predication plane. Therefore, it produces less accuracy in the source localization of radiation points. This will be discussed in the result analysis.

F. Error Divergence

The maximum reconstructed data has been treated as predicted touch source. Divergence between actual source and predicted source are computed as

$$\{p_{max}, p_x, p_y\} = \max(|Re[b_k(i,j)]|), \tag{41}$$

$$p_d = \sqrt{(t_x - p_x)^2 + (t_y - p_y)^2}, \tag{42}$$

where p_{max} , p_x , p_y , t_x and t_y denote respectively, the maximum of reconstructed data, maximum peak at x , y directions and ground sources. $Re[b_k(i,j)]$ is a real part of back propagated data. By using p_{max}, a maximum peak in reconstruction has been calculated for localizing the predicted source(p_d).

IV. Result Analysis

As per our previous discussion, the measurement position was set by the computing as (43)

$$N_s = (S_s * A_m)/\Delta^2, \tag{43}$$

where S_s is the total square meter of vibrating source, A_m is the maximum aperture size that we require for the hologram plane, Δ is the sensor spacing and N_s represents number of measurement positions.

In our experiment, source size (S_s) was $0.36 \ \ m^2$, measurement spacing was 0.02 m and maximum aperture size was the same as the source,i.e., $A_m = 1$. As far as hologram intensity is concerned the minimum wave length may be as twice as spatial resolution, i.e., $\lambda_{min} = 2 * \tau$. In addition, measured acoustic data set was obtained by the spatial discrete dimension so that we required minimum number of nodes per λ_{min}. This may be around $2\pi/\theta$ ($\theta = 60^o$) , i.e., it is a factor to ensure the satisfactory level of spatial resolution in the prediction. Thus, we utilized 900 $(0.36/0.02^2)$ measurement positions in the hologram plane. By using these computations, a experimentation set up was simulated for the result analysis. Fig.13 shows the result of prediction source and distance measures. It reveals that incorporation of complex k-space provided mean distance of ± 0.1802 cm in the prediction whereas the real k-space distance mean was ± 0.6766 cm. A larger distance of source prediction may cause the false alarm in the localization. Therefore, complex k-space caused better accuracy than real plane in the prediction.

A. Prediction of Unmeasured Data

As we retrieved unmeasured data from measured signals the estimated prediction data set was evaluated to determine its efficacy in back propagation. It was carried out by evaluating peak-signal to noise ratio (PSNR) between the measured and back propagated data sets. Fig. 14 shows various occurrence of prediction of unmeasured or reconstructed data and its MAC and PSNRs. Fig. 15 shows reconstruction errors and its residuals. In our experiment, an average of 12.5dB PSNR was obtained in the entire prediction process. It revealed that this approach afford well reconstruction than the real k-space method.

B. Changing Source Directions

We conducted four phases of experiments on unmeasured data to estimate the localization sources. During the first phase, we made x direction sources as fixed and altered in z sources sequentially by 0.15 cm. It produced mean distance of 0.1802 cm for the complex k-space and 0.6766 cm for the real k-space. The experiment result is depicted in Fig. 18. In second phase of experiment, z direction coordinates were fixed and x directions were changed, it provided that no mean distance change was in complex space but real space mean distance was 0.6115 cm. This is illustrated in Fig. 19.

Both x and z directions were altered in the third phase of experiment. Localizing mean distance of complex wavenumber

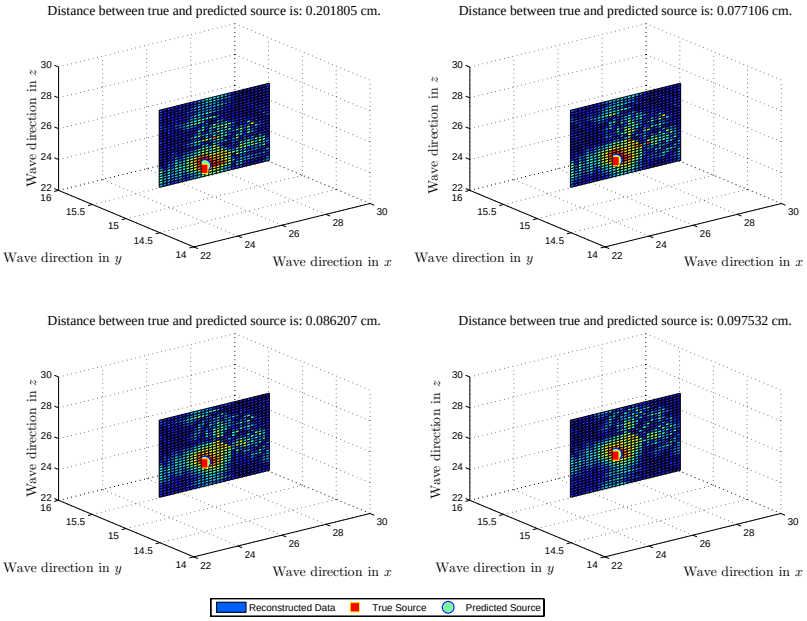

Fig. 13. Prediction of source and distance measures.

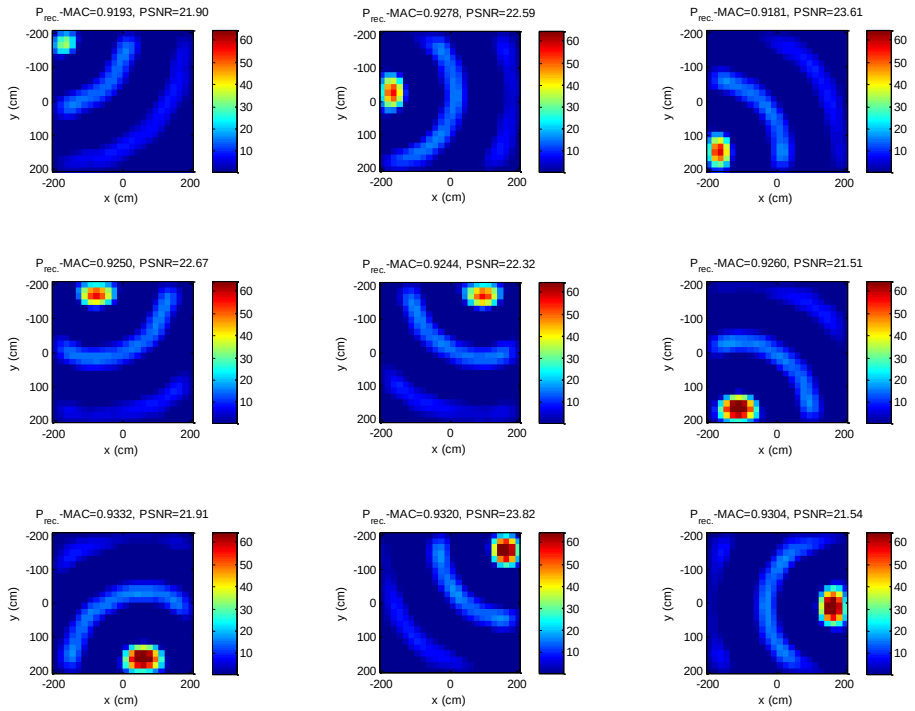

Fig. 14. Reconstructed pressure z_d = 0.2m, f = 400Hz.

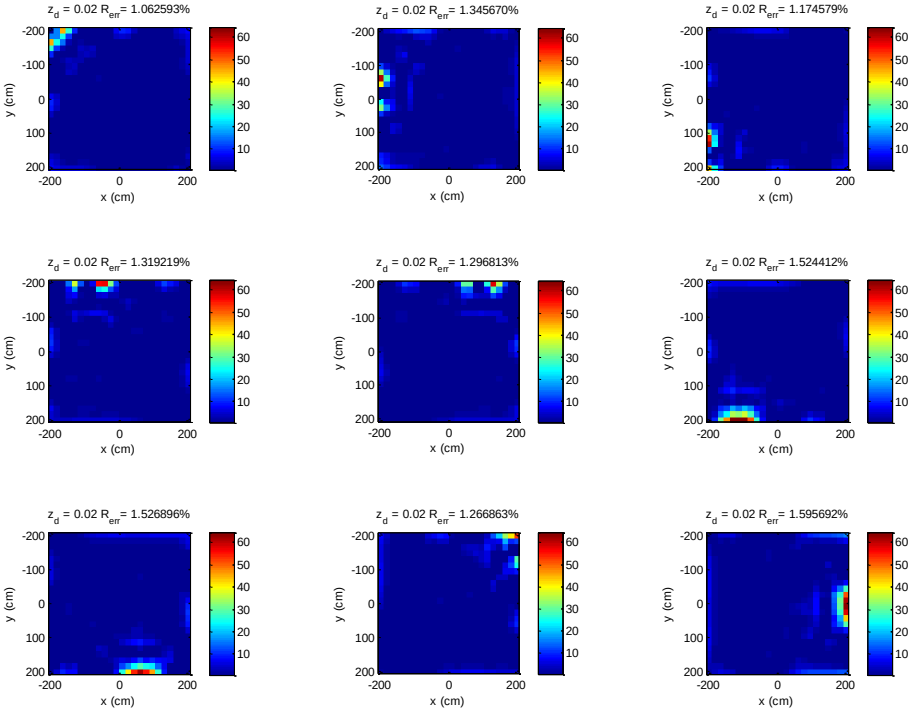

Fig. 15. Reconstruction error and its residuals on edges of the measurement plane.

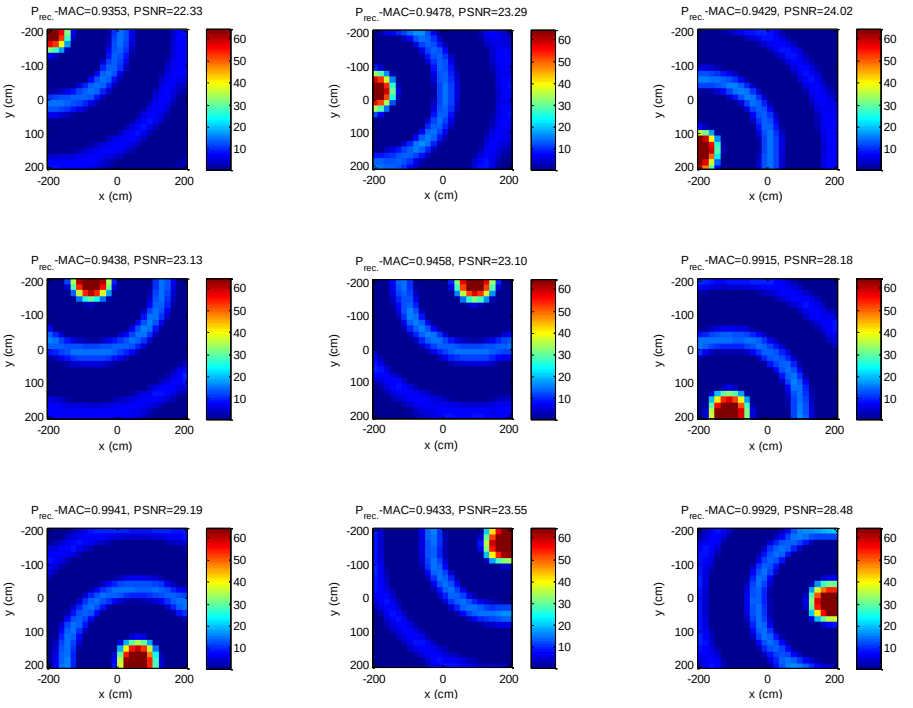

Fig. 16. Linear predictive based extrapolation and its reconstructed pressure z_d = 0.2m, f = 400Hz.

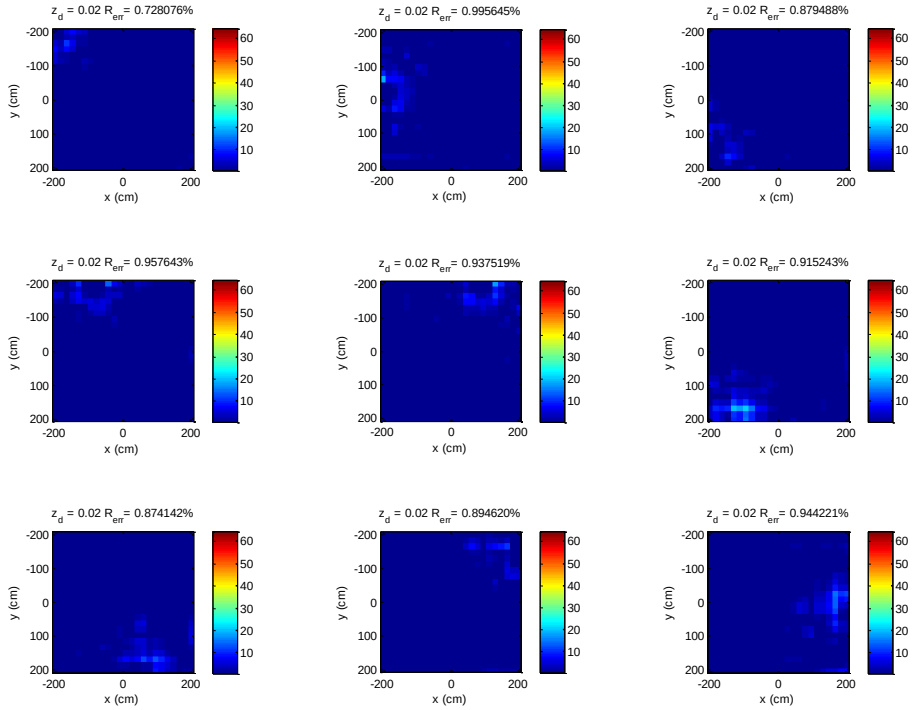

Fig. 17. Linear predictive based extrapolation reconstruction error and its residuals on edges of the measurement plane.

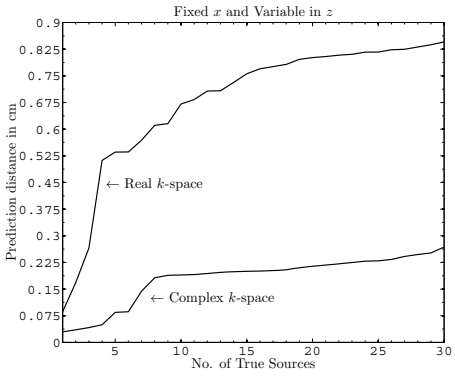

Fig. 18. Localizing distance in Prediction with fixed in x and variable in z.

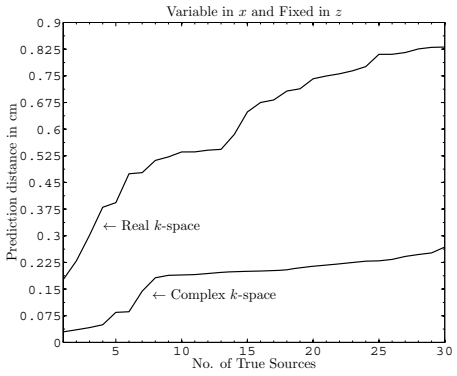

Fig. 19. Localizing distance in Prediction with fixed in z and variable in x.

was 0.1364 cm and real space was 0.5631 cm. Fig. 20 depicts the localization distance in prediction source by varying both directions. As compare to previous two phases, this phase provided improved localization mean distance. It was 0.1364 cm localizing distance. In the next phase of experiment, we prepared an experiment setup by randomly altering measurement spacing. The localizing mean distance was 0.1350 cm and 0.6170 cm in complex and real spaces, respectively. This is shown in Fig. 21. Table I tabulates the localization distances of four phases of experiments. Collectively, an average distance of 0.6168 cm in the real k-space and 0.1579 cm in the complex k-space were reported by our approach. From these experiments, we observed that incorporation of complex k-space in the wavenumber domain was found to be produced efficient localization in predicting the sources.

C. Discussion on Localization

Localization of active sources is an important work in this paper. Here, we have made a practice environment to simulate predicted distance by measuring single active frequency with zero-padding. During the transformation and back propagation the measured data were enveloped with complex k-space domain. As a result, considering complex plane produced an improved unmeasured data set as well as localization distance

was also efficiently minimized as compare to the real space. Spatial resolution is a core problem in the near acoustic holography, we utilized quite number of measurement positions according to the minimum wavelength and resolution. It is mainly due to evanescent waves that decay exponentially in diverge distance. In order to improve the spatial resolution in the hologram plane within the acoustic wavelength, it is essential to obtain measurements in the near field. So that we include evanescent waves in the back propagation process to achieve enhanced localization distance. In the case of evanescent wave, if real k-space was alone included in the back propagation then the wavenumber domain enveloped only for the propagating waves so that wavenumber propagation in the complex plane was abandoned from the predication plane, as a result, it produced less accurateness.

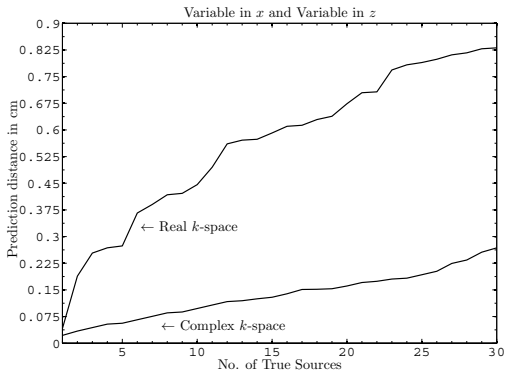

Fig. 20. Localizing distance in Prediction with variable in x and variable in z.

D. Further Research

This paper discloses more research options in the area of acoustic holography. Even though, we improved the discontinuity of signals and enhance the smooth transition of data from the source to hologram plane, a further research is required for improving the spectral resolution on wavenumbers before transforming into Fourier space. A problem of finite aperture can be minimized by increasing the spatial resolution based on predicting impulse responses from the known the response instead of synthesizing by zero impulses. Furthermore, an extrapolation algorithm is required to incorporate predicting impulses from its neighborhood pressure with 2D windowing. Here, we have employed 2D Tukey windowing with zero impulses extrapolation method. Main objective behind our method is to enhance the spatial resolution which intends to improve the accuracy of localization between true and predicted sources. However, due to high wavenumber artifacts, zero-padding may not enhance the spectral resolution in k-space. But expanding the N samples by n resulting $O(N + n \log N + n)$ computational complexity. Thus, we require a method to reduce the computational complexity and improve spectral resolution in k-space that is to be opted for reducing spectral leakage with less order of computation. On the other hand, instead of extrapolating the finite aperture edges and its derivatives, we can also interpolate or fill-up the breaches in the hologram aperture. This allows the use of several patches along the active-region-of-interest without equally distant rectangular measurement grids. Furthermore we require a spatial post processing on the predicted plane. It enhances the resolution after inverse propagation by means of applying filter over the prediction plane. This process could further improve the localization accuracy.

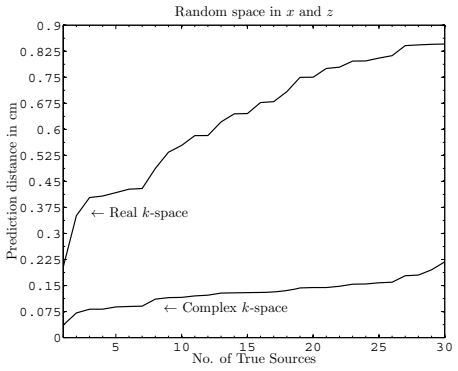

Fig. 21. Localizing distance in Prediction with random in x and z.

V. Conclusion

In this paper, a method of source localization based on complex k-space wavenumber was proposed. We simulated a empirical environment to predict the touch impacts. An incorporated complex k-space wavenumber was employed for the prediction process with zero-padding and 2D windowing. It is observed that complex k-space provided an improved accuracy in terms of predicting the sources rather than invoking only on real k-space. Furthermore, the reconstruction of prediction plane was also done to retrieve an enhanced version of the measured pressure. It assisted us to reinstate sufficient unmeasured data from the ill-posed data set. We studied that the problem of predicting unmeasured data has been resolved by the wavenumber complex plane and provided an average of 0.1579 cm localization distance between the true and predicted

TABLE I
Localization Accuracy in Distance

Phases of Experiments	Localization Distance(cm)	
	Real k-space	Complex k-space
Fix. x Var. z	0.6766	0.1802
Var. x Fix. z	0.6115	0.1802
Var. x Fix. z	0.5621	0.1364
Rad. x Rad. z	0.6170	0.1350
Mean distance	0.6168	0.1579

sources. Here, we resolved the finite aperture problem by zero-padding and windowing. However, an efficient exploration and interpolation approach will be required to enhance the removal of truncation effects transpiring on the finite aperture. This will prevent the requirement of huge measurements in the hologram plane therefore back propagation can be done with a smaller measurement data.

ACKNOWLEDGMENT

Author thank Asst. Prof. Andy W. H. Kong, Nanyang Technological University, Singapore for his suggestions to improve this research study in an extensive manner.

REFERENCES

[1] S. Rick, L. Ines, B. R. N, and N. Henk, "Truncated aperture extrapolation for fourier-based near-field acoustic holography by means of border-padding," *Journal of the Acoustical Society of America*, vol. 125(6), pp. 3844–3854, 2009.

[2] E. G. Williams and J. D. Maynard, "Holographic imaging without the wavelength resoultion limit," *Phys. Rev. Lett.*, vol. 45, pp. 554–557, 1980.

[3] J. D. Maynard, E. G. Williams, and Y. Lee, "Nearfield acoustic holography: I. theory of generalized holography and the development of nah," *J. Acoust. Soc. Am.*, vol. 78, pp. 1395–1413, 1985.

[4] E. G. Williams, *Fourier Acoustics: Sound Radiation and Nearfield Acoustical Holography*. Academic, London, 1999.

[5] S. F. Wu, "Methods for reconstructing acoustic quantities based on acoustic pressure measurements," *J. Acoust. Soc. Am.*, vol. 12, no. 5, pp. 2680–2697, Nov. 2008.

[6] J. Hald, "Basic theory and properties of statistically optimized near-field acoustical holography," *Journal of the Acoustical Society of America*, vol. 125(4), pp. 2105–2120, 2009.

[7] S. Kenji and U. Hiroshi, "Data extrapolation method for boundary element method based near-field acoustical holography," *Journal of the Acoustical Society of America*, vol. 115(2), pp. 785–796, 2004.

[8] Z. Wang and S. F. Wu, "Helmholtz equation-least-squares method for reconstructing the acoustic pressure field," *J. Acoust. Soc. Am.*, vol. 102, pp. 2020–2032, 1997.

[9] E. G. Williams, H. H. Brian, and C. H. Peter, "Fast fourier transform and singular value decomposition formulations for patch nearfield acoustical holography," *Journal of the Acoustical Society of America*, vol. 114(3), pp. 1322–1333, 2003.

[10] D. J. Chappell and P. J. Harris, "A burton-miller inverse boundary element method for nearfield acoustic holography," *Journal of the Acoustical Society of America*, vol. 126(1), pp. 149–157, 2009.

[11] R. Steiner and J. Hald, "Near-field acoustical holography without the errors and limitations casued by the use of spatial dft," *Int. J. Acoust. Vib.*, vol. 6, pp. 83–89, 2001.

[12] S. R. Woolston, "Development of methods to propagate energy density and predict farfield directivity using nearfield acoustic holography," *Master of Science thesis, Brigham Young University*, pp. 1–155, 2009.

[13] M. C. Harris and J. D. Blotter, "Obtaining the complex pressure field at the hologram surface for use in near-field acoustical holography when pressure and in-plane velocities are measured," *Journal of the Acoustical Society of America*, vol. 119(2), pp. 888–816, 2006.

[14] Y. H. Kim, "Acoustic holography(chapter 26)," *Springer Handbook of Acoustics*, vol. 10.1007/978-0-387-30425-0, pp. 1077–1099, 2007.

[15] A. J. Berkhout, "A holographic approach to acoustic control," *J.Audio Eng.Soc.*, vol. 36, pp. 977–995, 1988.

[16] E. G. Williams and J. D. Maynard, "Numerical evluation of rayliegh integral for planar acoustic radiators using the fft," *Journal of the Acoustical Society of America*, vol. 72(6), pp. 2020–2030, 1982.

[17] K. Saijyou and S. Yoshikawa, "Reduction methods of the reconstruction error for large-scale implementation of near-field acoustical holography," *H. Acoust. Soc. Am.*, vol. 110, no. 4, pp. 2007–2023, 2001.

[18] R. Bremananth, A. W. H. Khong, and A. Chitra, "Localizing acoustic touch impacts using zip-stuffing in complex k-space domain," *World Academy of Science, Engineering and Technology Journal*, vol. 60, pp. 1389–1395, 2011.

[19] B. Liu, R. Bremananth, and A. W. H. Khong, "A wavenumber-fitting extrapolation method for fft-based near-field acoistic holography using microphone array," *ICASSP2011, Prague*, pp. 145–148, 2011.

R Bremananth received the B.Sc and M.Sc. degrees in Computer Science from Madurai Kamaraj and Bharathidsan University in 1991 and 1993, respectively. He obtained M.Phil. degree in Computer Science and Engineering from GCT, Bharathiar University, in 2002. He received his Ph.D. degree in 2008 from Department of Computer Science and Engineering, PSG College of Technology, Anna University, Chennai, India. He has completed his Postdoctoral Research (PDF) in Information Engineering from the School of Electrical and Electronic Engineering, Information Engineering (Div.) at Nanyang Technological University, Singapore, 2011. He has 18+ years of experience in teaching, research and software development at various Institutions. Currently, He is an Assistant Professor in the Information Systems and Technology department, Sur University College, Sur, Oman, affiliated to Bond University Australia. He received the M N Saha Memorial award for the best application oriented paper in 2006 by Institute of Electronics and Telecommunication Engineers (IETE). His fields of research are acoustic imaging, pattern recognition, computer vision, image processing, biometrics, multimedia and soft computing.
Dr. Bremananth is a member of Indian society of Technical Education (ISTE), Advanced Computing Society (ACS), World Academy of Science, Engineering and Technology (WASET), International Association of Computer Science and Information Technology (IACIT) and IETE. He can be reached at bremresearch@gmail.com.